Numerical Investigation of Internal Flow Field for Diffuser Passage Compressor

Mai Yamagami ,Naoki Tsuchiya, Dai Kato, Hidekazu Kodama
IHI Corporation
229, Tonogaya, Mizuho-Machi, Nishitama-Gun, Tokyo, 190-1297, JAPAN

Kazuomi Yamamoto, Shunji Enomoto
Japan Aerospace Exploration Agency

Yasuo Horiguchi
Foundation for promotion of Japanese Aerospace Technology

Eisuke Outa
Waseda University

Keywords: Diffuser Passage, Tip clearance, Stall, CFD

Abstract

The influence of different grids on numerical prediction of subsonic compressor performance and stall was investigated. Two types of grids were examined, structured H type grid and structured O-H type grid. Evaluations were conducted by comparing the numerical results with experimental results obtained from a low-speed single-stage rig test for a new concept compressor, called diffuser passage compressor, aiming at improving tip clearance sensitivity.

At low mass flow operating conditions, the numerical calculation with O-H type grid showed that the lowest mass flow operating point for which the calculation was able to converge was almost the same as the lowest steady mass flow obtained from the rig test. On the other hand, the numerical calculation with structured H type grid diverged at higher mass flow operating point. It was found that this difference was attributed to the effect of double-valuedness of H type grid that existed at leading edge on the boundary layer development on the blade surface.

Introduction

Research and Technology Development in Japanese Environmentally Compatible Engine for Small Aircraft Project (Eco Engine Project) was started in 2003 as a seven-year project. The objective of this project is to improve engine system integration capability and to establish advanced technologies required for next generation aircraft engines, which are environmentally friendly and economically viable [1].

As an engine becomes smaller, tip clearance of the high pressure compressor (HPC) becomes larger relative to the blade height. The pressure rise decreases and the stall point moves to higher flow as the tip clearance relative to the blade height is increased. The blade heights in the rear stages of the ECO Engine HPC are so small that it is required to improve stall margin, efficiency and tip clearance sensitivity.

There have been many investigations on the use of aerodynamic sweep in transonic compressors to improve the performance and stability. For subsonic compressors, several attempts have been made to investigate the beneficial aspects of forward swept rotors. McNulty, et al [2] conducted an experimental and analytical evaluation of the impact of forward swept rotors on a low-speed model of the subsonic rear stages of a high-speed compressor. They demonstrated improvements in both efficiency and stall margin and reduced tip clearance sensitivity. Outa, et al [3] compared the performance of a conventionally stacked radial rotor with a forward swept rotor in a low-speed single-stage rig and showed that incorporation of forward sweep improved tip clearance sensitivity.

In the ECO Engine project, a new concept called Diffuser Passage (DP) Compressor, which also aims at improving tip clearance sensitivity by reducing tip clearance flow, was attempted. To demonstrate the concept, low-speed single-stage rig tests were performed installing DP and Conventional (CNV) compressors with different tip clearances to assess changes in tip clearance sensitivity [4][5]. In the rig tests, a significant improvement in tip clearance sensitivity was measured with the DP compressor.

Detailed CFD analyses were conducted to improve the understanding and interpretation of the test results of the new concept compressor. In the CFD analyses, two types of grids were used, one is structured H type grid which is widely used in the field of turbomachinery CFD because of its easy and fast grid generation, and another one is structured O-H type grid in which the grid orthogonality near the blade surface is ensured. The calculation results using the two types of grids were compared with the test results. This paper presents some new findings obtained from the investigation on influence of different grids on the prediction of compressor performance and stall.

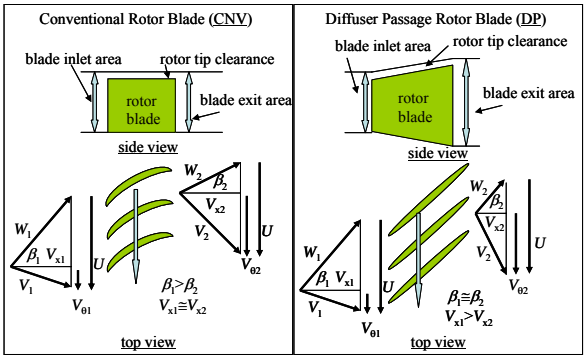

Figure 1 Concept of diffuser passage compressor

Concept of DP Compressor

Figure 1 compares the new concept compressor design with the conventional (CNV) design. In CNV, annular passage usually contracts toward downstream to keep axial velocity constant. Aerodynamic work is done by turning the relative flow across the rotor by airfoil camber. In DP rotor, annular passage expands, so the same work is done by axial velocity deceleration across the rotor with much less relative flow turning than in CNV. Since local acceleration by turning on the suction surface is suppressed, local large pressure difference across the blade is reduced. Therefore the tip leakage flow is expected to decrease considerably. DP rotor needs certain axial length as an annular diffuser. This results in longer chord and possibly higher solidity, which add to reduced pressure difference. Since higher solidity increases profile loss, a trade off exists with its decreasing effect of tip clearance loss.

Absolute flow angle at DP rotor exit becomes larger than that at CNV rotor exit, meaning DP stator needs to remove larger swirl than in CNV stator. However, its diffusion factor remains at the same level as that of CNV stator, since the annular passage contracts toward downstream in DP stator.

Test Compressor Configurations

Figure 3 shows the schematics of 1.5stage low speed compressor at Waseda University in two configurations, DP and CNV.

To compare the aerodynamic performance between CNV and DP rotor, two low-speed model rigs were designed with the same aerodynamic loading. The design parameters of both configurations are summarized in Table 1. As shown in Figure 2, blade surface velocity difference, i.e. surface pressure difference between suction and pressure surface is suppressed well in DP compared to CNV design. Down stream stator for each of the configuration was also designed to obtain same swirl angle and Mach number at the stage exit.

Table 1 DP and CNV rotor design specification

	DP	CNV
Flow codffiecient ϕ_1	0.49	0.49
work coefficient ψ_1	0.36	0.36
Pressure coeffiecitnt ψ_{t-t}	0.35	0.35
Turning	16	23
Solidity C/S	2.6	1.6
Aspect ratio	0.36	0.64
Diffusion factor	0.46	0.44
Number of rotor	31	33
Rotor tip Mach number	0.33	0.33

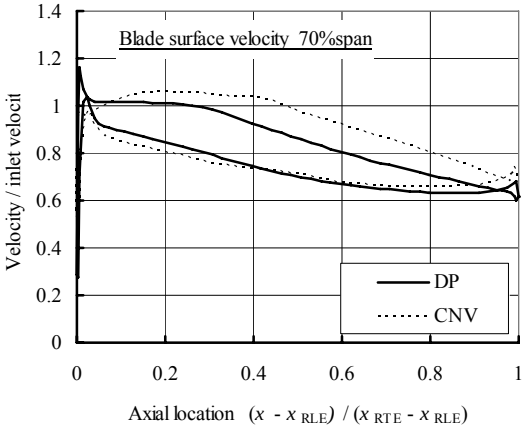

Figure 2 Design blade surface velocity distribution

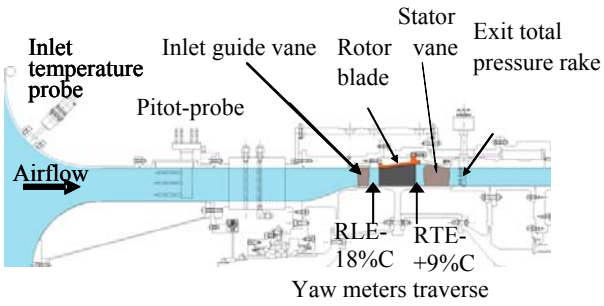

(a) Cross-sectional view of DP configuration

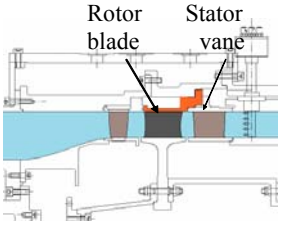

(b) CNV configuration

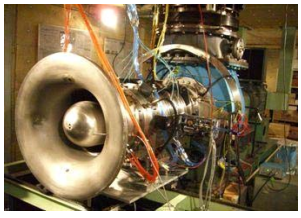

(C) External view of test compressor

Figure 3 Low speed compressor rig of DP and CNV models

The detail flow measurements were made in the rig test. Mass flow rate was measured by an inlet Pitot rake. Stage pressure rise was measured by the Pitot rake and exit pressure rakes. Rotor pumping and loss were measured by radial traverse of three-hole yawmeters

These pneumatic data were taken with pressure transducers of 0.1%accuracy of selected range. Wall pressure was taken by a transducer of 0.075%FS accuracy (GE DPI800). Unsteady rotor exit flow field was measured by hot-fiber-film probes (DANTEC 55R56&57).

Numerical Procedure

Computational Code

CFD code used in this study is UPACS. UPACS is a multi block Navier-stokes solver developed by JAXA [6][7]. The code was originally developed for the external flows, and then the code was extended to apply to internal flows in turbomachinery.

The governing equations are the time-dependent 3D Reynolds-Averaged Navier-Stokes equations. The convection fluxes are discretized by Roe's flux difference splitting with 3rd order MUSCL, and the viscous fluxes are discretized by 1st order central difference. The Spallart-Allmaras one equation model is adopted for turbulence model. Time integration is evaluated by 1st order implicit Euler method in local time step.

Computational Grid

Two types of grids, structured O-H type grid and structured H type grid were used in this study as shown in Figure 4. H type grid suits for blade to blade structured grid generation in turbomachinery, but has a grid singularity on the blade surface around the leading edge where discontinuity in some flow solutions is inevitable because of the double-valuedness at the singular point. O-H type grid in which O-topology is incorporated in the immediate vicinity of the blade surface eliminates the singularity and also guarantees a highly orthogonal grid on the blade surface.

Both O-H grid and H grid had 161 points in the streamwise direction and 121 points in the spanwise direction. In the pitchwise direction, O-H grid had 79 points for a total of about 1.8 million points and H grid had 129 points for a total of 2.5 million points..

In the O-H grid, the tip clearance region consisted of H-topology and O-topology. Both O-H grid and H-grid had 85 and 21 points in the chordwise and across the gap, respectively, in the tip clearance region. In radial direction, O-H grid had 43 points and H-grid had 33 points.

The numbers of grid points were determined by a grid dependency study.

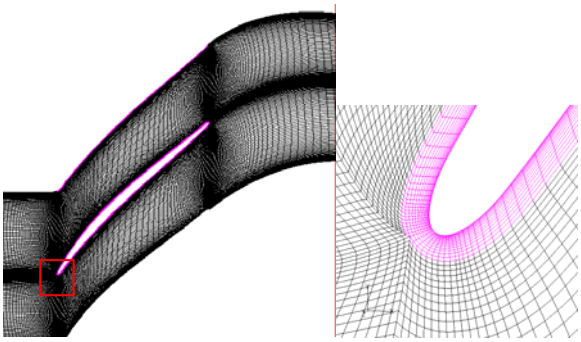

(a) Blade to blade mesh (b) Leading edge detail
Figure 4.1 O-H type grid

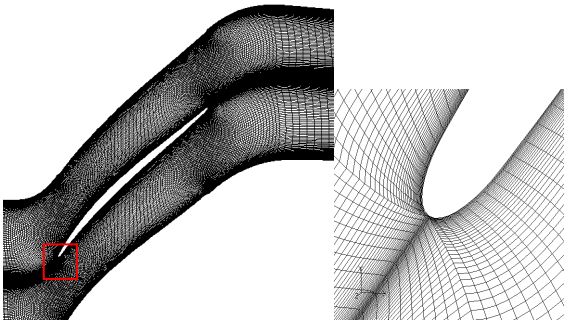

(a) Blade to blade mesh (b) Leading edge detail
Figure 4.2 H type grid

Boundary Conditions

In order to obtain empirically derived boundary conditions for the rotor CFD analysis, a through flow analysis was performed using measured data. In the through flow analysis, the loss of Inlet Guide Vane was estimated by CFD analysis, because it was not able to derive the loss from the various measurements in the rig test.

At the upstream boundary, the distribution of total temperature, total pressure and flow angles obtained from the through flow calculation results were fixed. Static pressure was fixed at the exit boundary. Non-slip and adiabatic wall boundary condition were applied to blade surface and hub/casing surfaces.

Results and Discussions

Overall Performance

In the rig test, the rotor rotation speed was held constant at design speed, while a throttle downstream of the exit scroll was changed to obtain rotor characteristics. Steady performance measurements were made at several throttle settings. The lowest flow point of the test data in Figure 5 is the last stable throttle position during the transient closure to stall.

In Figure 5, rotor characteristics obtained by CFD analysis using both O-H grid and H grid are compared with the test results. In the CFD analysis, the rotor characteristics were obtained by swinging the static pressure at outflow boundary from the test condition

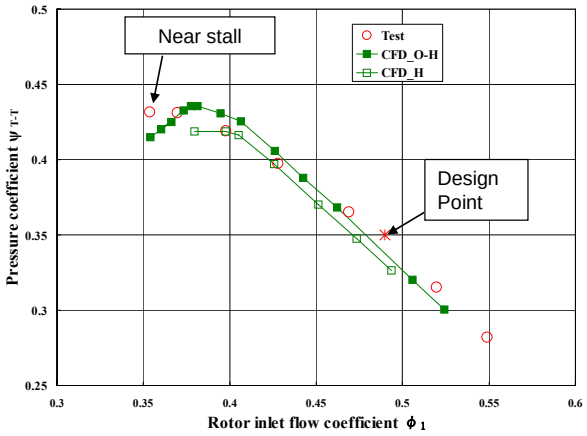

Figure 5 Comparison of computed performance with test data

near the design point, and the lowest flow point on the characteristics is the highest back pressure point for which the calculation was able to converge.

At higher flow rate than ϕ_1= 0.4, both CFD results show the same slope of the total pressure rise and reasonably agree with the test results. At lower flow rate than ϕ_1=0.4, measured characteristics in the rig test keeps negative slope of the total pressure rise until the last stable throttle position, while the calculated characteristics using O-H grid turn the slope to positive at around ϕ_1=0.37. However the lowest flow point on the characteristics obtained by CFD with O-H grid is almost the same as the last stable flow point in the rig test. On the other hand, the numerical calculation using H grid diverged at higher flow rate.

Axial distribution of casing wall static pressure

Figure 6 (a) shows the axial distribution of measured static pressure acquired from an array of pressure taps on the rotor tip casing wall at each flow rate. Although the profile of static pressure in the axial direction varies with the flow rate, a favourable pressure rise is obtained at all flow rates.

The axial distribution of wall static pressure on the rotor tip calculated by CFD with O-H grid is shown in Figure 6 (b) at each flow rate. The overall trend of the static pressure rise at each flow rate is well captured by the CFD prediction. At low flow rates, the calculation shows little static pressure rise around the trailing edge, but an endwall separation can not be seen in the calculations.

Figure 6 (c) compares the axial distribution of wall static pressure between numerical analyses and measurement at three flow rates. At flow rate near the design point and higher flow rate than design point, the CFD results using O-H grid and H grid show a reasonable agreement with the measurement, but the wall static pressure rises near the leading edge of both CFD results are lower than the test results at lower flow rate than design point. This indicates that, in the CFD prediction, the flow angle near the tip might be given at lower incidence than that in the real machine.

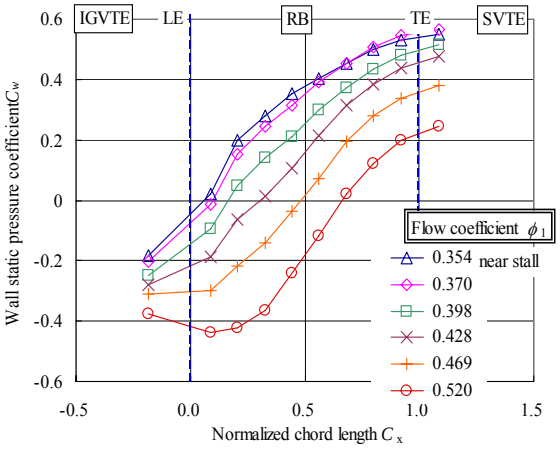

(a) Test data

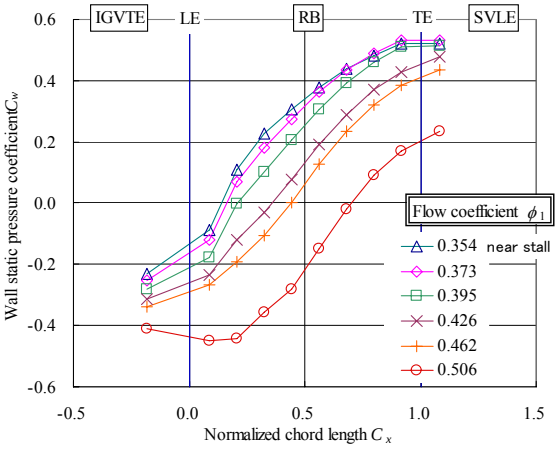

(b) Calculation (O-H type grid)

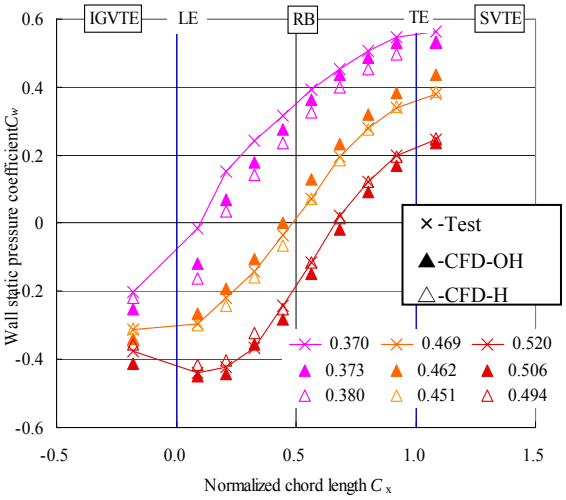

(C)Comparison between computed data and test data

Figure 6 Axial Distribution of Wall Pressure

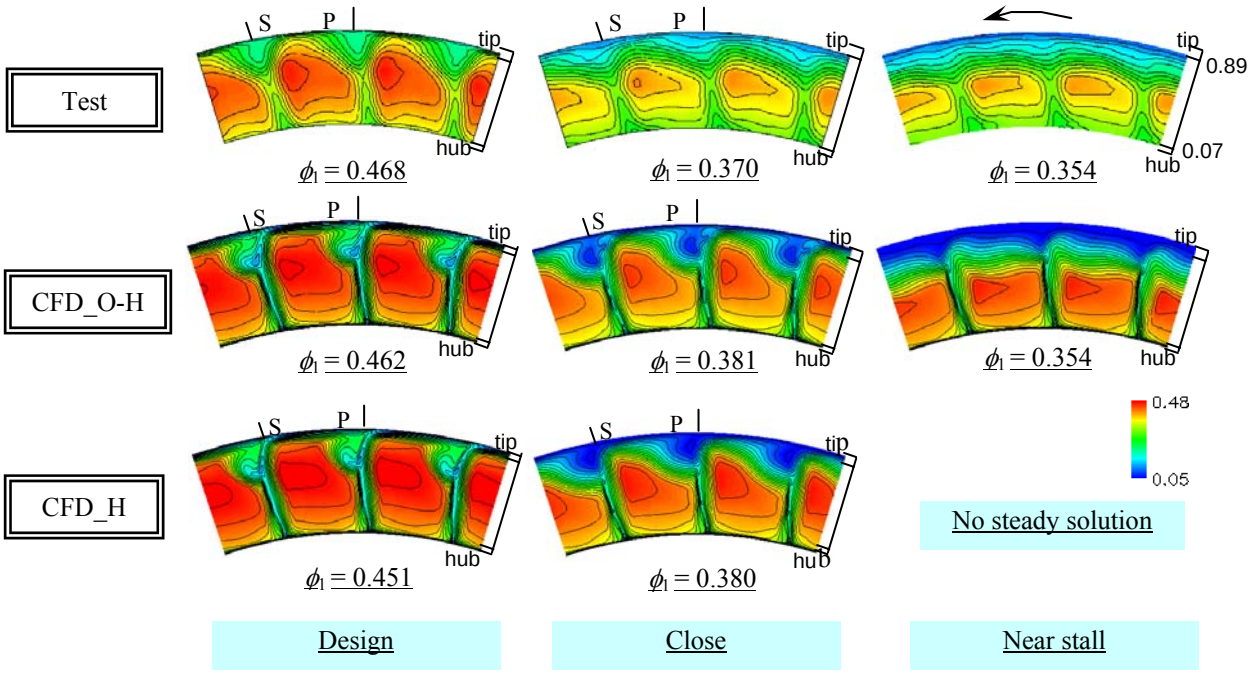

Figure 7 Comparison of Computed Rotor Exit Flow Field with Test Results (Axial Velocity V_x/U_{t1})

Contours of axial velocity at rotor exit

In Figure 7, computed contours of normalized axial velocity obtained by using both O-H grid and H grid are compared with hot-fiber film data at the rotor exit plane. In the figure, the comparisons are made at three flow rates, the flow rate near the design point ϕ_1=0.47, the lowest flow rate of CFD prediction with H grid ϕ_1=0.38 and the lowest flow rate of both measurements and CFD prediction with O-H grid ϕ_1=0.354.

Both CFD results capture overall features of axial velocity contours which can be observed in the measured contours, but the radial profiles of axial velocity are quite different from the measurements. The measured axial velocities in the main stream are lower than those of predictions, but near the casing endwall the measured axial velocities are higher at all flow rates. One of the possible reasons is that turbulent radial mixing took place in the real machine due to the unsteadyness produced by incoming wakes and endwall secondary flows of relatively rotating Inlet Guide Vanes, so that the momentum of endwall flow was strengthened.

Hoying, et al [8] suggested that a short length-scale rotating stall inception is a result of the motion of the tip clearance vortex moving forward of the blade row leading edge. The stall inception for this type of rotating stall occurs when the tip clearance vortex trajectory becomes perpendicular to the axial direction. In the CFD prediction with O-H grid at near stall ϕ_1=0.354, the tip clearance vortex trajectory is closer to perpendicular to the axial direction. It is considered that this resulted in the extension of low axial velocity region across the passage near the casing wall, as seen in Fig.7. Hoying, et al [8] also suggested that, when the tip clearance vortex trajectory becomes perpendicular to the axial direction, the position of tip clearance vortex becomes unstable. It is understandable that the divergence of solution occurred in the CFD calculation with O-H grid when throttled further from ϕ_1=0.354 might be attributed to this unstable condition.

In the case of rig test, a similar extension of low axial velocity fluid can be seen near the casing at ϕ_1= 0.354. Therefore it can be considered that the tip clearance vortex trajectory in the rig test was also closer to perpendicular to the axial direction at ϕ_1=0.354 and a short length-scale rotating stall inception occurred when the rotor was throttled further.

Computed axial velocity contour by H grid at the lowest flow rate ϕ_1=0.38 where the calculation was able to converge is similar to the contour predicted by O-H grid, except the low momentum core formed in the corner by the tip leakage flow. In the CFD results, the tip clearance vortex trajectory still lies further back in the blade passage at this flow rate. The divergence of solution occurred at lower flow rate than ϕ_1=0.38 is considered to be caused by different mechanism from in the CFD calculation with O-H grid.

Effect of grid generation type

Figure 8 compares the results of a streak line analysis between CFD calculation with O-H grid and H grid at ϕ_1=0.38. This flow rate is the last stable throttle position for CFD calculation with H grid, whereas the CFD calculation with O-H grid was able to obtain converged solutions at lower flow rate than

ϕ_1=0.38. However, there is no significant difference in flow structures associated with tip clearance flow between two CFD results.

Blade to blade contours of relative Mach number near leading edge are compared at 90 percent span and 50 percent span in Figure 10 and 11 respectively. In the contours of CFD results by H grid, flow discontinuities can be observed on the leading edge surface at both 90 and 50 percent spans. As mentioned before, this is due to double-valuedness at a singular point in the H grid. It can be seen that, because of the flow discontinuity, the boundary layer on the suction surface becomes thicker compared with the CFD results by O-H grid, and close to separation at 90 percent span.

At lower flow rate than ϕ_1=0.38, the boundary layer on the suction surface near the tip will separate in the CFD calculation with H grid. It may be possible that the divergence of solution occurred in the CFD calculation with H grid was related to this boundary layer separation.

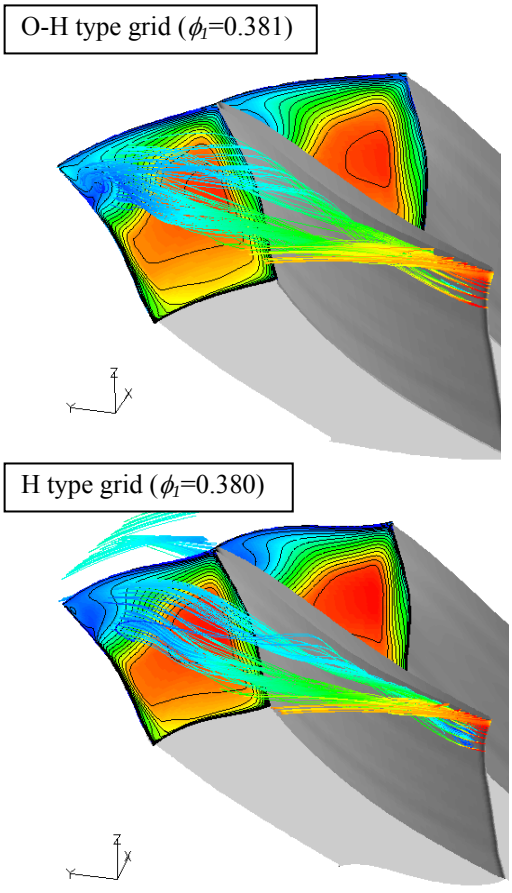

Figure 8 Comparison of Computed Streak lines between O-H type and H type grid

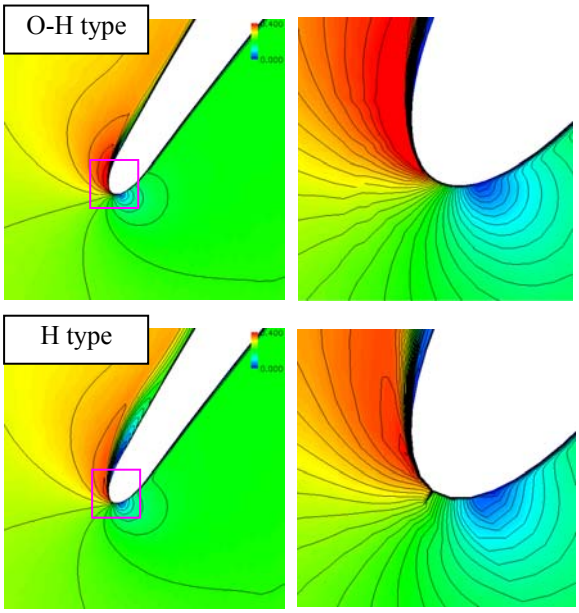

(a) Contours of Relative Mach number (b) Leading-edge detail

Figure 10 Comparison of Blade to blade contours of Relative Mach number between O-H type grid and H type grid at 90%span

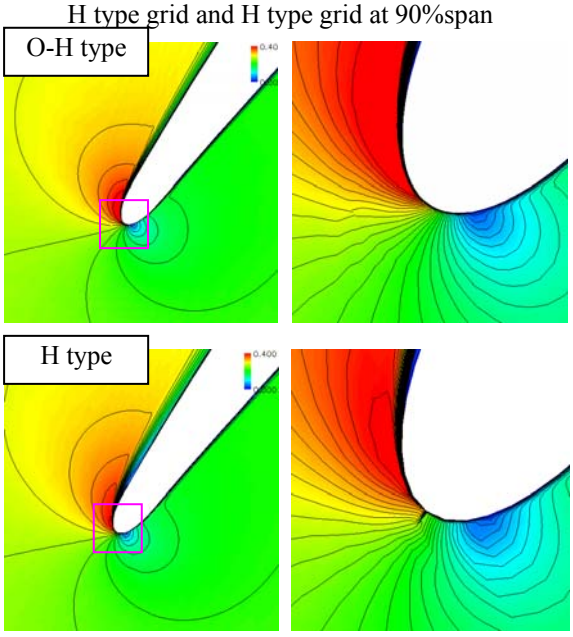

(a) Contours of Relative Mach number (b) Leading-edge detail

Figure 11 Comparison of Blade to blade contours of Relative Mach number between O-H type grid and H type grid at 50%span

Conclusion

In order to understand and interpret the low speed test results for a new concept compressor, numerical analyses were conducted using two types of grids, O-H type grid and H type grid.

1. Comparison between measured data and CFD results by O-H grid at the lowest stable flow rate indicates that a short length-scale rotating stall inception occurred in the rig test as a results of the motion of the tip clearance vortex moving forward of the blade passage.
2. The divergence of solution in the CFD calculation with O-H grid is thought to be attributed to unstable flow condition occurred when the tip clearance vortex trajectory becomes perpendicular to the axial direction.
3. The solution breakdown of CFD calculation with H grid is believed to relate to the effect of double-valuedness at a singular point in the H grid.

Acknowledgement

This study is conducted under the contract with New Energy and Industrial Technology Development Organization (NEDO) as part of the civil aircraft basic technology program of Ministry of Economy, Trade and Industry (METI)

Nomenclature

A	annulus area
A^*	flow passage area = $A\times\cos\beta$
C	chord length
Cp	specific heat at constant pressure
Cw	wall static pressure coefficient = $(P_{S,\,wall} - P_{T0}) / (P_{T1,\,R} - P_{S1})_a$
P	pressure
R	radius
T	temperature
U	rotor blade speed
V	absolute velocity
W	relative velocity
x	axial distance
β	relative flow angle
ε	tip clearance
ϕ	flow coefficient = $V_{x\,a}/U_t$
γ	specific heat ratio
ρ	air density
Ψ	work coefficient = $\mathrm{Cp}(T_{T2} - T_{T1}) / U_{t1}{}^2$
$\psi_{T\text{-}T}$	total pressure rise coefficient = $(P_{T2}-P_{T1})_a / \rho_{1\,a}U_{t1}{}^2$
$\psi_{S\text{-}S}$	static pressure rise coefficient = $(P_{S2}-P_{S1})_a / \rho_{1\,a}U_{t1}{}^2$
Cx	*normalized chord length* $=(X-X_{RLE})/C$

Subscripts

a	mass-weighed area average
M	mean or average
R	relative
RLE	rotor leading edge
RTE	rotor trailing edge
S	static
SP	stall point
T	total
t	rotor tip
x	axial component
wall	casing wall
θ	tangential component
0	compressor inlet
1	rotor inlet
2	rotor exit

Reference

(1) Funatogawa, O., 2005, "Research and Technology Development in Japanese Environmentally Compatible Engine for Small Aircraft Project," ISABE-2005-1010.

(2) McNulty, G. S., et al, 2004, "The Impact of Forward Swept Rotors on Tip Clearance Flows in Subsonic Axial Compressors," *ASME Journal of Turbomachinery*, Vol. 126, pp.445-454.

(3) Outa, E., 2006, "Rotating Stall and Stall-Controlled Performance of a Single Stage Subsonic Axial Compressor," *Journal of Thermal Science*, Vol.15, No.1, pp.1-13.

(4) Kato, D., et al, 2007, "Development of Diffuser Passage Compressor concept for small aircraft engines," ISABE 2007.

(5) Kato, D., et al, 2007, "Development of Diffuser Passage Compressor for Improved Performance Robustness against Tip-Clearance Flows," IGTC Tokyo 2007.

(6) Yamane, T., Yamamoto, K., Enomoto, S., Yamazaki, H., Takaki, R., and Iwamiya, T., "Development of A Common CFD Platform – UPACS -," Proc. Parallel CFD 2000 Conf., Elsevier Science, pp. 257-264., 2001.

(7) Takaki, R., et.al, "The Development of he UPACS CFD Environment," High Performance Computing, Proceedings of ISHPC 2003, Springer, p. p. 307-319, 2003.

(8) Hoying,D.A., Tan, C.S., Vo, H.D., and Greitzer, E.M., 1998, "Role of Blade Passage Flow Structures in Axial Compressor Rotating Stall Inception," ASME Paper No. 98-GT-588